Learning rate collapse prevents training recurrent neural networks at scale

Bariscan Kurtkaya, Mehmet Harmanli[*] *KUIS AI, Koc University, Istanbul, Turkey*

Alperen Cimen[*]**, Andy Alexander, Nina Miolane, Fatih Dinc**[†]
UC Santa Barbara, California, USA

Yucel Yemez[†] *KUIS AI, Koc University, Istanbul, Turkey*

Editors: List of editors' names

Abstract

Recurrent neural networks (RNNs) are central to modeling neural computation in systems neuroscience, yet the principles that enable their stable and efficient training at large scales remain poorly understood. Seminal work in machine learning predicts that the effective learning rate should shrink with the size of feedforward networks. Here, we demonstrate an analogous phenomenon, termed *learning rate collapse*, in which the maximum trainable learning rate decreases inversely with the number of neurons[1]. This behavior can be mitigated partially by scaling parameters with the inverse of network, though learning still takes longer for larger networks. These limits are further compounded by severe memory demands, which together make training large RNNs both unstable and computationally costly. As a proof of principle for mitigating learning rate collapse, we study the learning process of low-rank networks, which enforces a low-dimensional geometry in RNN representations. These results situate learning rate collapse within a broader lineage of scaling analyses in RNNs, with potential solutions likely to come from future work that incorporates careful consideration of symmetry and geometry in neural representations.

Keywords: Recurrent neural networks, computational neuroscience

1. Introduction

Recent advances in optical recording have enabled neuroscientists to measure the activity of tens of thousands to millions of neurons simultaneously (Ebrahimi et al., 2022; Bruzzone et al., 2021; Ahrens et al., 2013; Stringer et al., 2019). This capability to record large-scale neural activity has reinforced and expanded our understanding of *population coding*, *i.e.*, the principle that information is represented not by single units but by the collective dynamics of neural populations (Yuste, 2015; Baeg et al., 2003; Meyers et al., 2008; Chaudhuri et al., 2019; Averbeck et al., 2006). To investigate how these collective representations support diverse computations and to study neural circuitry, computational neuroscientists regularly train recurrent neural networks (RNNs) either as digital twins of recorded neural activity or on neuroscience-inspired tasks, utilizing methods from dynamical systems theory, topology, and geometry (Rajan et al., 2016; Perich and Rajan, 2020; Duncker and Sahani, 2021; Kurtkaya et al., 2025; Mante et al., 2013; Sussillo et al., 2015; Finkelstein et al., 2021; Sussillo and Barak, 2013).

[*] Equal contribution, order decided based on best of three soccer video games.
[†] Co-supervision, order decided based on seniority
1. Github code for reproducibility.

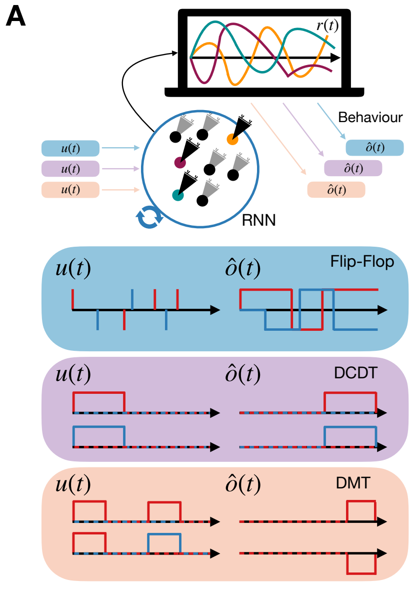

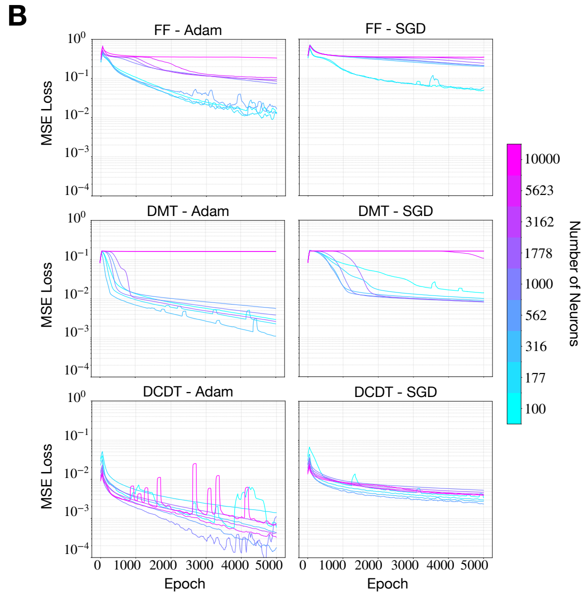

Figure 1: **Scaling the learning rate slows down training in all settings. (A)** Schematic of the three benchmark tasks: the flip-flop task (FF), the delayed cue discrimination task (DCDT), and the delayed match-to-sample task (DMT) (see Sec. 2.1). **(B)** In total, we trained 3,900 RNNs across tasks, learning rates, optimizers, and seeds. For network sizes greater than 100, we show the best-performing loss curves averaged across seeds. Larger networks consistently converge more slowly, since lower learning rates are required for stability. The learning rates (LR) are reported in Table 1.

With rank-constraints on RNNs, one can map the neural computations performed by large populations of neurons to low-dimensional internal latent variables (Mastrogiuseppe and Ostojic, 2018; Beiran et al., 2021; Valente et al., 2022) and study the neural algorithms implemented to solve specific tasks (Dubreuil et al., 2022). Building on this line of work, Dinc et al. (2025a) has developed a theoretical framework to characterize population-level dynamics at scale in an architecture-agnostic manner. However, even when using these interpretable methods, a fundamental gap exists between experimental and computational capabilities. While experimentalists can record from millions of neurons, most computational studies remain limited to networks with only a few hundred neurons (Masse et al., 2019; Yang et al., 2019; Kurtkaya et al., 2025). This discrepancy raises a critical question: What prevents artificial models from scaling to the same dimensions as their biological counterparts?

One well-known limitation is the sheer computational cost and memory demand. For an RNN with N neurons, the number of synaptic weights grows with $O(N^2)$, making it infeasible to simulate networks approaching the millions of units observed in biology. Yet computational burden alone does not fully explain the scaling barrier. A more fundamental issue arises from the optimization dynamics: analyses of gradient propagation in feedforward networks show that the variance of weight updates grows with network size, requiring the learning rate to scale inversely with N (Saxe et al., 2013; Gilboa et al., 2019; Yang et al., 2022). Without such adjustments of the learning rate, large networks are known to diverge rapidly during training.

In this work, we demonstrate an analog of this phenomenon in RNNs, which we term *learning rate collapse*. To establish this result, we systematically trained RNNs on three established memory tasks: the flip-flop task (FF), the delayed cue discrimination task (DCDT), and the delayed match-to-sample task (DMT) (see Fig. 1 and Sec. 2.1). We then quantified scaling laws by identifying the largest learning rates capable of training more than half of the model instances, which revealed a clear dependence on N (see Fig. 2, 3 and Sec. 3.1, 3.2). We then showed that scaling the recurrent weight matrices with N mitigates the learning rate collapse, but larger networks still take longer to train at the same learning rates (see Fig. 4 and Sec. 3.3). Importantly, while both strategies prevent divergence, they do so at the cost of significantly slowing learning, with larger networks requiring many more epochs to converge (see Fig. 1, 4). To overcome these limitations, we study a restricted training paradigm, in which the latent dynamical systems within low-rank RNNs are optimized (see Fig. 5 and Sec. 3.4). Conceptually, this corresponds to training the parameters at the level of population codes rather than the connections between individual neurons, though the former does describe the latter. While this approach is one possible method for mitigating the learning-rate collapse while simultaneously reducing memory and computational demands, further work incorporating geometry and symmetry in learned representations may be able to further decrease the number of parameters that need to be trained, thereby enabling training of large-scale RNNs.

2. Methods

2.1. Task details

In this work, we focus on three commonly studied short-term memory tasks from systems neuroscience literature (Masse et al., 2019; Yang et al., 2019; Sussillo and Barak, 2013).

The delayed cue discrimination task (DCDT) is a widely used paradigm for probing short-term memory in both biological and artificial neural networks (Kurtkaya et al., 2025). Each trial consists of three phases: an input phase T_{in}, during which a brief cue is presented; a delay phase T_{delay}, where no external input is provided and the RNN must internally maintain the cue; and a response phase T_{resp}, in which the RNN is required to produce an output based on the earlier cue. This structure makes DCDT a canonical framework for testing the ability to store and retrieve information across a silent interval. Formally, DCDT can be expressed as:

$$u(t) = \begin{cases} (0,1) \text{ or } (1,0), & \text{if } t \in T_{\text{in}}, \\ (0,0), & \text{otherwise}, \end{cases} \qquad o^*(t) = \begin{cases} u(T_{\text{in}}), & \text{if } t \in T_{\text{resp}}, \\ (0,0), & \text{otherwise}. \end{cases} \tag{1}$$

where $u(t)$ denotes the input at time t and $o^*(t)$ denotes the ground-truth output at time t.

The delayed match-to-sample task (DMT) has two cues T_{in_1} and T_{in_2} separated by a delay interval T_{delay}. RNN must determine whether they are identical or different and output the decision within the response window T_{resp}. Unlike simple DCDT, DMT requires both the maintenance of the first cue during the delay and its comparison to the second cue, making it a more demanding test of memory mechanisms. Formally, DMT can be expressed as:

$$u(t) = \begin{cases} (0,1) \text{ or } (1,0), & \text{if } t \in \{T_{\text{in}_1}, T_{\text{in}_2}\}, \\ (0,0), & \text{otherwise}, \end{cases}$$
$$o^*(t) = \begin{cases} +1, & \text{if } t \in T_{\text{resp}} \text{ and } u(T_{\text{in}_1}) = u(T_{\text{in}_2}), \\ -1, & \text{if } t \in T_{\text{resp}} \text{ and } u(T_{\text{in}_1}) \neq u(T_{\text{in}_2}) \\ (0,0), & \text{otherwise.} \end{cases} \tag{2}$$

where $u(t)$ denotes the input at time t, and $o^*(t)$ denotes the ground-truth output at time t ($+1$ for match, -1 for non-match, and 0 otherwise).

The flip-flop (FF) task has no explicit delay component. At each timestep, a cue may appear with some probability, either repeating the previous value or switching to the opposite ($+1$ or -1). The RNN must preserve its current state when the cue is unchanged and flip its output when the cue switches. This makes FF a test of continual state maintenance under unpredictable inputs, rather than storage across fixed delay intervals.

2.2. Recurrent neural networks

We focused on vanilla recurrent neural networks (RNNs) as models for studying population dynamics during short-term memory tasks. The recurrent dynamics were defined as

$$\tau \dot{r}(t) = -r(t) + \phi\left(W r(t) + W^{\text{in}} u(t)\right), \tag{3}$$

where $r(t) \in \mathbb{R}^N$ denotes the activity of N recurrent units (firing rates) at time t, $W \in \mathbb{R}^{N \times N}$ is the recurrent weight matrix, $W^{\text{in}} \in \mathbb{R}^{N \times d_{\text{in}}}$ is the input projection from d_{in}-dimensional external inputs $u(t)$. The nonlinear activation function $\phi(\cdot)$ was chosen as the hyperbolic tangent, $\phi(x) = \tanh(x)$, consistent with prior work on dynamical systems analyses of RNNs (Sussillo and Barak, 2013; Mastrogiuseppe and Ostojic, 2018). The time constant τ was fixed to unity without loss of generality. The network output was given by a linear readout of the recurrent state:

$$\hat{o}(t) = W^{\text{out}} r(t), \tag{4}$$

where $W^{\text{out}} \in \mathbb{R}^{d_{\text{out}} \times N}$ maps the recurrent activity into a d_{out}-dimensional output space. Training was performed by minimizing the mean squared error (MSE) between predicted and target outputs:

$$\mathcal{L} = \frac{1}{T} \sum_{t=1}^{T} \left\| \hat{o}(t) - o^*(t) \right\|^2, \tag{5}$$

where $o^*(t)$ denotes the task-specific target output and T is the trial length. Optimization was carried out with the Adam or SGD optimizer, depending on the experiment, across a range of learning rates and random seeds. Further details can be found in the Appendix or the Github codebase accompanying this paper.

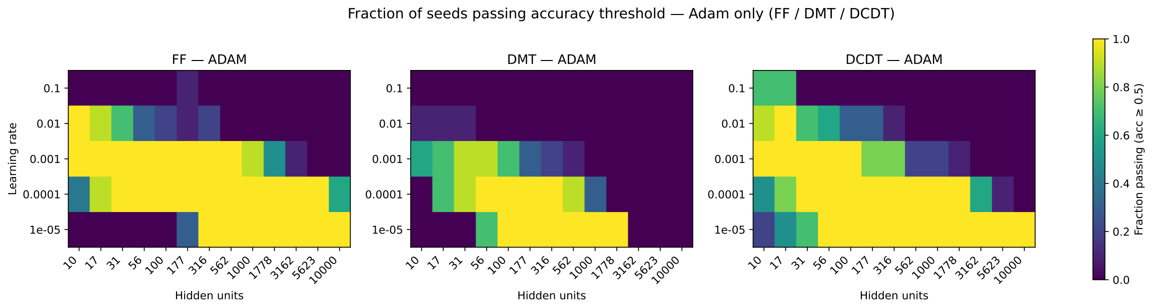

Figure 2: **Decreasing the learning rate is necessary for training larger networks.** We trained RNNs with 13 different sizes (10^1 to 10^4, evenly sampled on a log scale), 5 learning rates (10^{-1} to 10^{-5}, log-spaced), and 10 random seeds on three neuroscience tasks. After training, models were deemed successful if they achieved an accuracy greater than 0.5. We then plot the fraction of successful models across all tasks. The results reveal a clear negative scaling law: larger networks require proportionally smaller learning rates (consistent with the predicted $1/N$ behavior) to train successfully. For details see Table 2.

3. Results

3.1. Learning rate collapse prevents training large RNNs to perform short-term memory tasks

We first evaluated whether larger recurrent networks could be trained to perform the three memory tasks (Fig. 1A, Sec. 2.1). We trained RNNs using Adam and SGD across varying sizes and a wide range of learning rates, number of neurons, and seeds, resulting in 3,900 distinct networks (see Table 2). Moreover, Table 1 reports the best-performing learning rates for each setting, while Fig. 1B shows representative training curves averaged over seeds. The results revealed a consistent pattern: larger networks converged more slowly, and in many cases, learning rates that were effective for smaller models caused divergence or unstable dynamics in larger ones. Only by decreasing the learning rate were we able to restore stable optimization. Across all three tasks and both optimizers, this dependency on network size was robust: the number of recurrent units strongly determined the range of learning rates under which training remained stable. In other words, convergence of large recurrent networks requires systematically smaller learning rates and more training epochs. We termed this phenomenon as the “learning rate collapse.”

3.2. Quantifying the learning rate collapse

To quantify how learning rates scale with network size, we deemed models successful if they achieved an accuracy greater than 0.5. After classifying models, we computed the fraction of successful runs across seeds (Figure 2). From these results, we identified the largest learning rate that trained at least 50% of runs successfully for each network size. We then

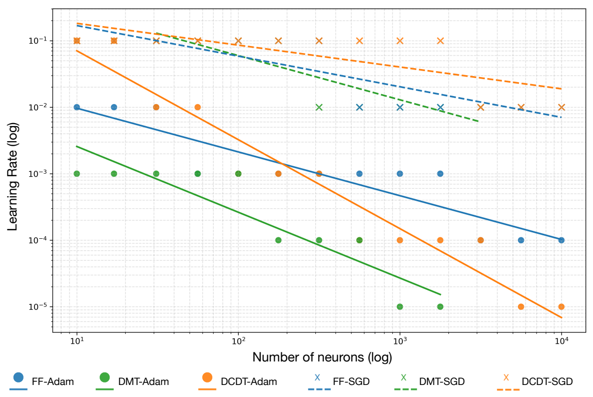

Figure 3: **Learning rate scales as $1/N$.** We fit a line to the largest learning rates at each network size that successfully trained at least half of the models. The resulting fits reveal a negative power-law scaling of the form N^β with $\beta < 0$. Estimated exponents: *FF-Adam,* $\beta = -0.66$*; DMT-Adam,* $\beta = -0.99$*; DCDT-Adam,* $\beta = 1.34$*; FF-SGD,* $\beta = -0.46$*; DMT-SGD,* $\beta = -0.66$*; DCDT-SGD,* $\beta = -0.33$.

fitted a power-law function to these critical learning rates:

$$\min_{a,\beta} \sum_i \left(\log_{10} LR_i - \left(a + \beta \log_{10} N_i\right)\right)^2 \quad \Rightarrow \quad LR = 10^a N^\beta, \tag{6}$$

where β is the slope and a is the intercept. Across all tasks and optimizers, the fitted curves exhibited a consistent decaying trend, demonstrating a negative power-law relationship between network size and the maximum stable learning rate (Figure 3). This result confirmed the existence of a scaling law: as N increased, the effective learning rate diminished following N^β with some $\beta < 0$. In fact, earlier work on feedforward networks suggests (and Figure 3 is consistent with this) that $\beta \approx -1$ is expected. Then, this raises an important question: as demonstrated in Figure 1, decreasing the learning rate slows down the training process; can rescaling the network parameters instead of rescaling the learning rate mitigate this slowdown?

3.3. Rescaling the parameters with network size mitigates learning rate collapse, but larger networks still require more epochs to train.

To test whether learning rate collapse could be alleviated by re-parameterizing, we defined a variant of the RNN in which both recurrent and output weights were rescaled with network size, *e.g.*, $W \to W/N$. This was inspired by the known results in feedforward networks (Yang et al., 2022), which practically ensured that the recurrent interactions, *i.e.*, $Wr(t)$, remained scale-invariant as the number of units increased. This formulation maintains the overall structure of the standard RNN update equation while it is expected to mitigate the theoretical N^{-1} scaling in the learning rate.

We trained rescaled RNNs of varying hidden dimensions on the 3-bit flip-flop task, using multiple learning rates and random seeds. Figure 4 shows the resulting loss trajectories

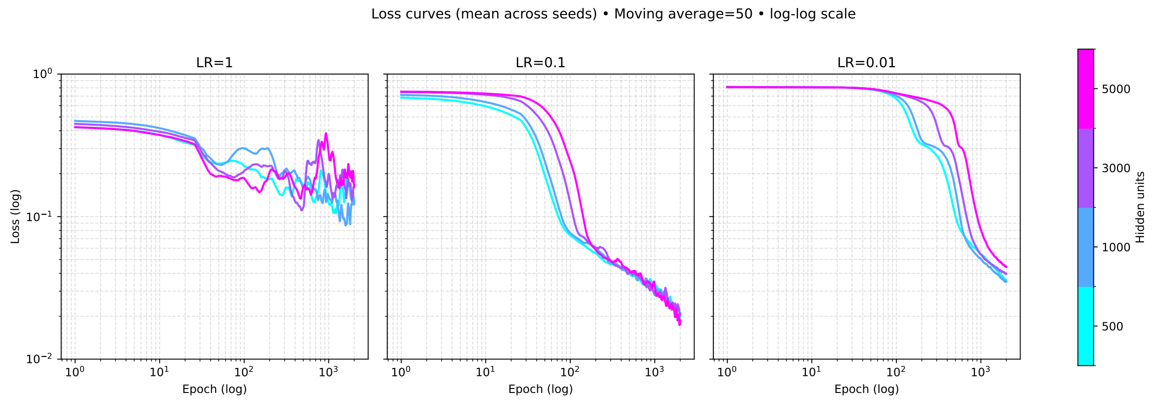

Figure 4: **Rescaling the parameters mitigates the learning rate collapse, but larger networks still take longer to train.** We defined the recurrent and output weights following a rescaling of the parameters, *i.e.*, $W \to W/N$, and retrained RNNs with varying sizes on the 3-bit flip-flop tasks. All RNNs failed to solve the task at the same learning rate, $LR = 1$, whereas for smaller learning rates, smaller networks learned the task faster. Each solid line is a mean over 5 runs, RNNs learn to perform the 3-bit flip flop tasks with a high accuracy ($> 90\%$) at around MSE ≈ 0.06. For details see Table 3.

across epochs. At high learning rates ($LR = 1$), all models failed to converge regardless of size, consistent with the instability induced by overly large parameter updates. At smaller learning rates, rescaling prevented divergence across network sizes, but convergence dynamics still differed systematically: smaller networks reached low loss values in relatively few epochs, whereas larger networks required substantially more iterations to achieve comparable accuracy (note the log-scale for the x-axis in Figure 4). In other words, parameter rescaling stabilized training but did not remove the disadvantage stemming from the scale when training these RNNs.

3.4. Learning low-rank representations alleviated the learning difficulties in large RNNs

While re-parameterization stabilized training, it did not remove the slowdown in large RNNs. We now show that a more effective strategy is to reformulate the dynamics in a low-rank structure that naturally supports scale-free learning. Specifically, we parametrized low-rank RNNs as

$$\tau \dot{r}(t) = -r(t) + \phi\left(\frac{1}{N}\sum_{k=1}^{K} m^{(k)} n^{(k)T} r(t) + W^{\text{in}} u(t)\right), \tag{7}$$

where $m^{(k)}, n^{(k)} \in \mathbb{R}^N$ are the embedding and encoding vectors for the k-th rank component, and K is the rank of the recurrent connectivity. Prior work has employed this factorization (referred to as "LINT" (Valente et al., 2022)). For this network, we can directly reduce the

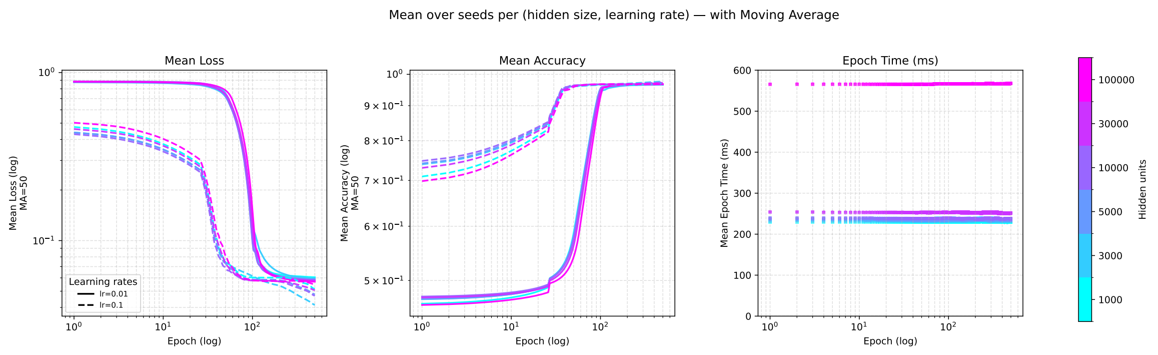

Figure 5: **Training low-dimensional latent representations (LPUs) mitigated the learning difficulties in large RNNs.** We trained low-rank RNNs to perform a 1-bit FF task ($K = 1$). Regardless of the network size, the learning progression curves looked nearly identical for all network sizes (left and middle). More importantly, most networks took about 250ms per epoch (except for the one with $100,000$ neurons, which likely required substantial memory), and about $O(100)$ epochs, training in about a minute. For details see Table 4.

dynamics into the latent system following:

$$\kappa_k(t) = \frac{1}{N} n^{(k)T} r(t). \tag{8}$$

The dynamics can be written entirely in terms of $\kappa_k(t)$:

$$\tau \dot{\kappa}_k(t) = -\kappa_k(t) + \frac{1}{N} n^{(k)T} \phi \left(\sum_{\ell=1}^{K} m^{(\ell)} \kappa_\ell(t) + W^{\text{in}} u(t) \right). \tag{9}$$

This latent formulation evolves only K variables rather than N, reducing the parameter count from $O(N^2)$ to $O(NK)$ compared to a full-rank network. Moreover, this can also be seen as a “deep” RNN with few neurons (with activities $\kappa(t)$) and a single high-dimensional hidden layer, with the extra interpretation that it can be mapped to a shallow RNN with many neurons (with activities $r(t)$) but a low-dimensional population code ($\kappa(t)$).

We trained these networks to perform a 1-bit FF task in Fig. 5, where removing the extra trainable dimensions enabled efficient training of very large networks. Strikingly, the training curves across network sizes collapsed onto nearly identical trajectories for a given learning rate, and even networks with 100,000 neurons converged within about a minute. Thus, low-rank training not only mitigated learning rate collapse but also achieved genuine scale-free performance in large RNNs, which is crucial for simulating or training virtual twins based on large-scale recordings.

4. Discussion

In this work, we identified *learning rate collapse* as an obstacle to training large RNNs. Across a range of short-term memory tasks, optimizers, and hyperparameters, we consistently found that the maximum trainable learning rate decreased with network size. This scaling law implies that stable training of larger RNNs requires progressively smaller learning rates, which in turn slows convergence and increases computational costs. Parameter rescaling partially stabilized training by normalizing the effective recurrent strength across network sizes. However, while this prevented divergence, it did not remove the slowdown: larger networks continued to require substantially more iterations to converge.

A low-rank latent formulation offered a simpler but useful solution. Projecting the dynamics into a reduced latent space decreased the parameter count from $O(N^2)$ to $O(NK)$, while preserving the expressive capacity of the network for the admittedly very simple 1-bit FF task that could be solved with only a rank-one RNN. In this setting, learning curves across network sizes collapsed onto one another, and even networks with 100,000 neurons trained efficiently within minutes. These findings suggest that enforcing low-dimensional structure may be a practical mechanism for scaling RNN training in a size-independent manner, though a lot more needs to be understood about limitations of learning in low-dimensional dynamical systems.

Taken together, our study situates learning rate collapse within the broader landscape of scaling laws in machine learning. Prior work has established width-dependent rescaling in feedforward networks; here we demonstrate that recurrent architectures face analogous constraints that manifest as a collapse of the effective learning rate. At the same time, our results resonate with recent neuroscience findings: large biological populations appear to implement computations through low-dimensional manifolds. One reason for this may be that learning becomes faster (though not necessarily easier, see (Dinc et al., 2025b)) when constrained to low-dimensional dynamical systems.

Limitations

Our work is rather preliminary in scope and therefore not without several limitations. First, we have not studied the effects of initialization in this work, which is very well known to impact the training process. Instead, we focused on a common initialization scheme that is used in practice (see the accompanying code). Second, extending our analysis to deep and/or gated RNNs and transformer-based recurrent models will clarify whether collapse is universal across sequence-processing architectures. Third, incorporating symmetry and geometry into parameterizations may yield additional scale-free formulations, complementing the low-rank approach. Finally, connecting these optimization limits to experimental data can shed light on how biological networks circumvent collapse, for example by exploiting structured connectivity, local learning rules, or population-level redundancy.

Reproducibility and code availability

Please refer to the Appendices and the accompanying Github, which is made publicly available with this paper in https://github.com/bariscankurtkaya/LR_Collapse_Neurips25.

References

Misha B Ahrens, Michael B Orger, Drew N Robson, Jennifer M Li, and Philipp J Keller. Whole-brain functional imaging at cellular resolution using light-sheet microscopy. *Nature methods*, 10(5):413–420, 2013.

Bruno B Averbeck, Peter E Latham, and Alexandre Pouget. Neural correlations, population coding and computation. *Nature reviews neuroscience*, 7(5):358–366, 2006.

EH Baeg, YB Kim, K Huh, I Mook-Jung, HT Kim, and MW Jung. Dynamics of population code for working memory in the prefrontal cortex. *Neuron*, 40(1):177–188, 2003.

Manuel Beiran, Alexis Dubreuil, Adrian Valente, Francesca Mastrogiuseppe, and Srdjan Ostojic. Shaping dynamics with multiple populations in low-rank recurrent networks. *Neural Computation*, 33(6):1572–1615, 2021.

Matteo Bruzzone, Enrico Chiarello, Marco Albanesi, Maria Elena Miletto Petrazzini, Aram Megighian, Claudia Lodovichi, and Marco Dal Maschio. Whole brain functional recordings at cellular resolution in zebrafish larvae with 3d scanning multiphoton microscopy. *Scientific reports*, 11(1):11048, 2021.

Rishidev Chaudhuri, Berk Gerçek, Biraj Pandey, Adrien Peyrache, and Ila Fiete. The intrinsic attractor manifold and population dynamics of a canonical cognitive circuit across waking and sleep. *Nature neuroscience*, 22(9):1512–1520, 2019.

Fatih Dinc, Marta Blanco-Pozo, David Klindt, Francisco Acosta, Yiqi Jiang, Sadegh Ebrahimi, Adam Shai, Hidenori Tanaka, Peng Yuan, Mark J Schnitzer, et al. Latent computing by biological neural networks: A dynamical systems framework. *arXiv preprint arXiv:2502.14337*, 2025a.

Fatih Dinc, Ege Cirakman, Yiqi Jiang, Mert Yuksekgonul, Mark J Schnitzer, and Hidenori Tanaka. A ghost mechanism: An analytical model of abrupt learning. *arXiv preprint arXiv:2501.02378*, 2025b.

Alexis Dubreuil, Adrian Valente, Manuel Beiran, Francesca Mastrogiuseppe, and Srdjan Ostojic. The role of population structure in computations through neural dynamics. *Nature Neuroscience*, pages 1–12, 2022.

Lea Duncker and Maneesh Sahani. Dynamics on the manifold: Identifying computational dynamical activity from neural population recordings. *Current opinion in neurobiology*, 70:163–170, 2021.

Sadegh Ebrahimi, Jérôme Lecoq, Oleg Rumyantsev, Tugce Tasci, Yanping Zhang, Cristina Irimia, Jane Li, Surya Ganguli, and Mark J Schnitzer. Emergent reliability in sensory cortical coding and inter-area communication. *Nature*, 605(7911):713–721, 2022.

Arseny Finkelstein, Lorenzo Fontolan, Michael N Economo, Nuo Li, Sandro Romani, and Karel Svoboda. Attractor dynamics gate cortical information flow during decision-making. *Nature Neuroscience*, 24(6):843–850, 2021.

Dar Gilboa, Bo Chang, Minmin Chen, Greg Yang, Samuel S Schoenholz, Ed H Chi, and Jeffrey Pennington. Dynamical isometry and a mean field theory of lstms and grus. *arXiv preprint arXiv:1901.08987*, 2019.

Bariscan Kurtkaya, Fatih Dinc, Mert Yuksekgonul, Marta Blanco-Pozo, Ege Cirakman, Mark Schnitzer, Yucel Yemez, Hidenori Tanaka, Peng Yuan, and Nina Miolane. Dynamical phases of short-term memory mechanisms in RNNs. In *Forty-second International Conference on Machine Learning*, 2025. URL https://openreview.net/forum?id=ybBuwgOPOd.

Valerio Mante, David Sussillo, Krishna V Shenoy, and William T Newsome. Context-dependent computation by recurrent dynamics in prefrontal cortex. *nature*, 503(7474): 78–84, 2013.

Nicolas Y Masse, Guangyu R Yang, H Francis Song, Xiao-Jing Wang, and David J Freedman. Circuit mechanisms for the maintenance and manipulation of information in working memory. *Nature neuroscience*, 22(7):1159–1167, 2019.

Francesca Mastrogiuseppe and Srdjan Ostojic. Linking connectivity, dynamics, and computations in low-rank recurrent neural networks. *Neuron*, 99(3):609–623, 2018.

Ethan M Meyers, David J Freedman, Gabriel Kreiman, Earl K Miller, and Tomaso Poggio. Dynamic population coding of category information in inferior temporal and prefrontal cortex. *Journal of neurophysiology*, 100(3):1407–1419, 2008.

Matthew G Perich and Kanaka Rajan. Rethinking brain-wide interactions through multi-region 'network of networks' models. *Current opinion in neurobiology*, 65:146–151, 2020.

Kanaka Rajan, Christopher D Harvey, and David W Tank. Recurrent network models of sequence generation and memory. *Neuron*, 90(1):128–142, 2016.

Andrew M. Saxe, James L. McClelland, and Surya Ganguli. Exact solutions to the nonlinear dynamics of learning in deep linear neural networks. *arXiv preprint arXiv:1312.6120*, 2013. URL https://arxiv.org/abs/1312.6120.

Carsen Stringer, Marius Pachitariu, Nicholas Steinmetz, Charu Bai Reddy, Matteo Carandini, and Kenneth D Harris. Spontaneous behaviors drive multidimensional, brainwide activity. *Science*, 364(6437):eaav7893, 2019.

David Sussillo and Omri Barak. Opening the black box: low-dimensional dynamics in high-dimensional recurrent neural networks. *Neural computation*, 25(3):626–649, 2013.

David Sussillo, Mark M Churchland, Matthew T Kaufman, and Krishna V Shenoy. A neural network that finds a naturalistic solution for the production of muscle activity. *Nature neuroscience*, 18(7):1025–1033, 2015.

Adrian Valente, Jonathan W Pillow, and Srdjan Ostojic. Extracting computational mechanisms from neural data using low-rank rnns. *Advances in Neural Information Processing Systems*, 35:24072–24086, 2022.

Greg Yang, Edward J Hu, Igor Babuschkin, Szymon Sidor, Xiaodong Liu, David Farhi, Nick Ryder, Jakub Pachocki, Weizhu Chen, and Jianfeng Gao. Tensor programs v: Tuning large neural networks via zero-shot hyperparameter transfer. *arXiv preprint arXiv:2203.03466*, 2022.

Guangyu Robert Yang, Madhura R Joglekar, H Francis Song, William T Newsome, and Xiao-Jing Wang. Task representations in neural networks trained to perform many cognitive tasks. *Nature neuroscience*, 22(2):297–306, 2019.

Rafael Yuste. From the neuron doctrine to neural networks. *Nature reviews neuroscience*, 16(8):487–497, 2015.

Table 1: Best learning rates (α) for each task, optimizer, and network size N demonstrated in Figure 1.

N	FF-Adam	FF-SGD	DMT-Adam	DMT-SGD	DCDT-Adam	DCDT-SGD
100	10^{-3}	10^{-1}	10^{-4}	10^{-2}	10^{-3}	10^{-1}
177	10^{-3}	10^{-1}	10^{-4}	10^{-2}	10^{-4}	10^{-1}
316	10^{-3}	10^{-1}	10^{-4}	10^{-2}	10^{-4}	10^{-1}
562	10^{-3}	10^{-2}	10^{-5}	10^{-2}	10^{-4}	10^{-2}
1000	10^{-4}	10^{-2}	10^{-5}	10^{-2}	10^{-5}	10^{-2}
1778	10^{-4}	10^{-2}	10^{-5}	10^{-2}	10^{-5}	10^{-2}
3162	10^{-4}	10^{-2}	10^{-1}	10^{-2}	10^{-5}	10^{-2}
5623	10^{-4}	10^{-2}	10^{-2}	10^{-2}	10^{-5}	10^{-2}
10000	10^{-5}	10^{-2}	10^{-3}	10^{-3}	10^{-5}	10^{-2}

Appendix A. Methods

Low-rank RNNs approximation:
To reduce the dimensionality of recurrent dynamics while preserving essential computations, we employed a low-rank approximation of the recurrent connectivity matrix. Specifically, instead of maintaining a full recurrent weight matrix $W \in \mathbb{R}^{N\times N}$, where N denotes the number of recurrent units, we factorized it into a dot product of two low-rank matrices:

$$W \approx \sum_{i=1}^{K} m_i n_i^T, \tag{10}$$

where $m \in \mathbb{R}^{N\times K}$ and $n \in \mathbb{R}^{K\times N}$, with $K \ll N$. This factorization enforces a rank-K constraint on the recurrent connectivity, ensuring that the dynamics are confined to a K-dimensional latent subspace. To illustrate this low-rank approximation, we can define the following:

$$\kappa(t) = n^T\, r(t), \quad \kappa(t) \in \mathbb{R}^K, \tag{11}$$

where $r(t) \in \mathbb{R}^N$ denotes the high-dimensional recurrent state of the network and $\kappa \in \mathcal{R}^K$ denotes the latent representations. Here, n is the *encoding weights* projecting population activity into the low-dimensional latent subspace (constrained by low-rank approximation).

Training with low-rank RNNs:
We trained a rank-one RNN, parametrized through low rank factorization of the reconnectivity matrix, and propagated in low-dimensional space (*i.e.,* latent space) rather than

evolving it in high-dimensional full neural state vectors (*i.e.,* RNN's update equation). More specifically, we employed following time evolution method to train our large networks:

$$\tau\dot{\kappa}(t) = -\kappa(t) + \frac{1}{N} n^T \tanh(m\kappa(t) + W^{\text{in}} u(t)). \tag{12}$$

Here, N denotes the total number of neurons in the recurrent population, m represents the embedding weights, and n the encoding weights. The task input at time t is denoted by $u(t)$, with W^{in} specifying the input weight matrix.

The networks were trained using the mean squared error (MSE) as the loss function, and model parameters were optimized with the Adam optimizer. Mean accuracy (Fig. 5**B**) was assessed by computing the correlation coefficient between predicted and target trajectories and averaged out across various trials using PyTorch's built-in *correlation-coefficient* method. In addition, we recorded the computational cost of training per epoch (Fig. 5**C**) by measuring the elapsed time during execution using Python's *time* module.

Training Setups:
We trained recurrent neural networks (RNNs), with dynamics governed by a leaky integration update and nonlinearity tanh. Training hyperparameters were as follows for all experiments:

Table 2: Training setups for learning rate collapse RNN experiments.

Parameter	**Specification**
Random seeds	10 independent runs per configuration
Learning rates	$\{10^{-5}, 10^{-4}, 10^{-3}, 10^{-2}, 10^{-1}\}$
Batch size	50 trials during training; 200 trials for evaluation/analysis
Epochs	5,000 epochs (all runs completed; no adaptive early stopping)
Optimizers	Adam and SGD (default torch parameters), with mean squared error (MSE) loss
Network sizes	13 Hidden dimensions sampled logarithmically between 10^1 and 10^4
Network Initializations	Xaiver Uniform for W, W_{in}, W_{out}
Computational resources	Parallelized cluster jobs (up to 100 processes). Training executed primarily on CUDA GPUs (H100 NVL/RTX 3090); small-scale runs on CPU. Epoch runtime measured with Python `time` module.

Table 3: Training setups for our weight rescaling RNN experiments.

Parameter	**Specification**
Random seeds	5 independent runs per configuration
Learning rates	$\{10^{-2}, 10^{-1}, 10^{0}\}$
Batch size	50 trials during training; 50 trials for evaluation/analysis
Epochs	2,000 epochs (all runs completed; no adaptive early stopping)
Optimizers	Adam (default torch parameters), with mean squared error (MSE) loss
Network sizes	$\{500, 1000, 3000, 5000\}$
Network Initializations	Xaiver Uniform for W, W_{in}, W_{out} and $1/N$ scaling in the W, W_{out}
Computational resources	Parallelized cluster jobs. Training executed primarily on CUDA GPUs (H100 NVL/RTX 3090); small-scale runs on CPU. Epoch runtime measured with Python `time` module.

Table 4: Training setups for our LPU RNN experiments.

Parameter	**Specification**
Random seeds	5 independent runs per configuration
Learning rates	$\{10^{-2}, 10^{-1}\}$
Batch size	50 trials during training; 50 trials for evaluation/analysis
Epochs	500 epochs (all runs completed; no adaptive early stopping)
Optimizers	Adam (default torch parameters), with mean squared error (MSE) loss
Network sizes	$\{10^3, 3*10^3, 5*10^3, 10^4, 3*10^4, 10^5\}$
Network Initializations	Xaiver Uniform for m, n - Normal Distribution for W_{in}, W_{out}
Computational resources	Parallelized cluster jobs. Training executed primarily on CUDA GPUs (RTX 3090). Epoch runtime measured with Python `time` module.

Rescaling Procedure

A key challenge in scaling recurrent neural networks lies in the growth of activity magnitudes with network size. The contribution of the recurrent weights to the hidden state can be written as a dot product

$$(W_{\text{rec}} h_t)_i \;=\; \sum_{j=1}^{N} W_{\text{rec}}^{(i,j)}\, h_t^{(j)}, \tag{13}$$

where each hidden unit i accumulates input from N presynaptic units. Similarly, the output readout is given by

$$(W_{\text{out}}h_t)_k \;=\; \sum_{j=1}^{N} W_{\text{out}}^{(k,j)}\, h_t^{(j)}. \tag{14}$$

As N increases, these summations scale with the number of terms, leading to larger effective magnitudes. Without correction, this growth destabilizes training and forces the learning rate to shrink approximately as $1/N$ to maintain stability.

To counteract this effect, we applied a rescaling procedure in which both recurrent and output weights were normalized by network size:

$$W_{\text{rec}} \;\to\; \frac{W_{\text{rec}}}{N}, \qquad W_{\text{out}} \;\to\; \frac{W_{\text{out}}}{N}. \tag{15}$$

This normalization ensures that the total contribution of recurrent interactions and output projections remains approximately constant as N increases, rather than diverging with the number of units. By contrast, the input projection

$$(W_{\text{in}}u_t)_i \;=\; \sum_{m=1}^{d_{\text{in}}} W_{\text{in}}^{(i,m)}\, u_t^{(m)}, \tag{16}$$

only sums over the input dimensionality d_{in}, which is fixed and independent of the hidden size N. Therefore, its magnitude does not grow with N, and there is no need to normalize W_{in}. Similarly, biases are additive constants and do not scale with network size, so they were also left unmodified.

Statistical treatment: To assess training outcomes, we evaluated performance across multiple random seeds for each configuration. A run was classified as *successful* if it achieved accuracy above 0.5 (chance level for binary discrimination tasks). We then computed the *success density*, defined as the fraction of seeds that met this threshold. This measure provided a robust estimate of training reliability for each setting. Critical learning rates were identified as the largest learning rates at which at least 50% of runs succeeded, enabling power-law fits across network sizes.